Article

Hydrogen Generation by Nickel Electrodes Coated with Linear Patterns of PTFE

Alion Alushi [1,2] , Atheer Al-Musawi [1] , Kyuman Kim [1], Chong-Yong Lee [1], Klaudia Wagner [1] and Gerhard F. Swiegers [1,*]

[1] Intelligent Polymer Research Institute, University of Wollongong, Wollongong, NSW 2522, Australia; alion.alushi@smail.th-koeln.de (A.A.); kyuman@uow.edu.au (K.K.)

[2] Cologne Institute for Renewable Energy (CIRE), Faculty of Process Engineering, Energy and Mechanical Systems, TH Köln, Betzdorfer Str. 2, 50679 Köln, Germany

[*] Correspondence: swiegers@uow.edu.au

Abstract: Previous studies have shown that partially coating electrode surfaces with patterns of 'islands' of hydrophobic tetrafluoroethylene (PTFE; Teflon) may lead to more energy efficient gas generation. This occurred because the gas bubbles formed preferentially on the PTFE, thereby freeing up the catalytically active metallic surfaces to produce the gas more efficiently. This work examined electrochemically induced hydrogen bubble formation on a nickel electrode surface that had been coated with linear patterns of PTFE. The impact of the PTFE line size (width) and degree of coverage was examined and analyzed. No improvement in electrical energy efficiency was observed up to 15 mA/cm^2 when comparing the PTFE-coated electrodes with the control bare uncoated electrode. However, increasing PTFE coverage up to 15% generally improved electrolysis performance. Moreover, samples with 50% wider lines performed better (at the equivalent PTFE coverage), yielding an overpotential decline of up to 3.9% depending on the PTFE coverage. A 'bubble-scavenging' phenomenon was also observed, wherein bubbles present on the PTFE lines rapidly shrunk until they disappeared.

Keywords: hydrogen; electrolysis; efficiency; PTFE; overpotential; bubbles

1. Introduction

The world has, for decades, been shifting energy production away from fossil fuels toward renewable energy (RE), the potential of which is yet to be fully exploited. Technical, economic, and socio-political aspects, all of which are interconnected, have challenged the establishment of RE in the energy market [1–5]. Therefore, many strategies and measures have been taken to overcome the challenges in these fields.
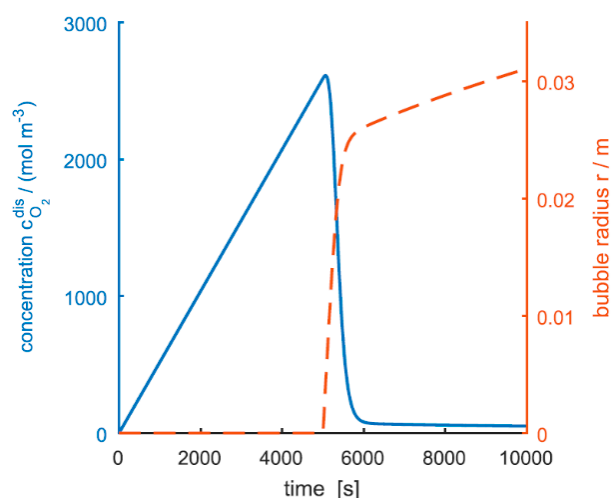
One of the main strategies to maximize the use of RE has been the development of energy storage systems [6]. The most common types of energy storage technologies are mechanical, thermal, and electrochemical in character [5,7,8]. Hydrogen, on which this work focuses, is an energy carrier that can be produced in RE-powered electrochemical cells and which can be stored in large amounts in geological formations like salt caverns under the Earth's surface [9]. Renewable hydrogen of this type, also called 'green hydrogen', can be used as fuel and feedstock for industrial applications (for example, in the chemical and steel industries [10,11]) and could also be used in the future in heavy transport applications such as maritime and aviation propulsion [12].

Green hydrogen, which is hydrogen produced from water using electrolysis that is powered by RE, effectively serves as a store of renewable energy, i.e., a renewable fuel. As with all processes involving energy conversion, a critical feature of green hydrogen is the energy efficiency with which it can be produced during electrolysis [13]. Present-day commercial electrolyzers are inefficient at producing green hydrogen, leading to poorly

efficient energy storage compared to batteries [14]. Attempts to increase the reaction efficiency by using expensive platinum-group metals (PGMs) have caused higher electrolyzer costs [15–17].
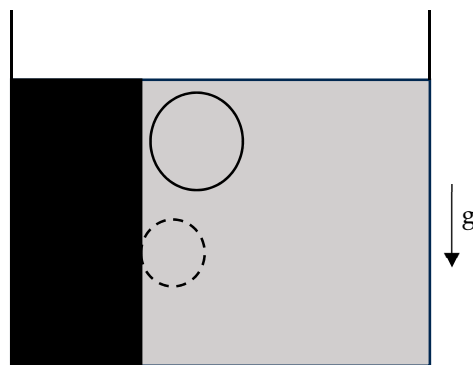
Key losses that occur during electrolysis arise from the formation of gas bubbles and their presence on electrode surfaces and in the electrolyte. Both hydrogen and oxygen are produced in the form of gas bubbles that reduce the overall efficiency of the process. The bubbles block the active surface area by masking the electrode, thereby leading to ohmic overpotentials (due to blocking of the ionic pathways between the anode and cathode) as well as activation overpotentials (due to blocking of the chemical reactions) [18,19]. Therefore, keeping the electrode surface and the inter-electrode space free of gas bubbles is essential for the realization of highly efficient electrolyzers and competitive hydrogen prices in the energy market [20,21].

Understanding bubble mechanics is key to developing strategies to improve electrolytic performance. Bubble formation is known to go through four stages [20], namely nucleation, growth, detachment, and the mass transport of bubbles away from the electrodes and out of the inter-electrode space. The newly formed gas molecules at the electrodes (e.g., hydrogen molecules) are not only poorly soluble in water, but they also exhibit low diffusion constants [22]. As a result, newly formed gas has no way to escape the electrode and instead supersaturates the electrolyte around the electrodes, with concentrations growing as high as 125–350 times the saturation concentration before gas bubbles start nucleating [23–25]. The need to achieve these supersaturation levels represents inefficiencies in the gas production process [24,25]. Once a bubble has nucleated, it may grow by coalescence with other bubbles or by gas diffusion into the bubble, with gas concentrations around it in the solution falling to near-saturation concentration, as shown in Figure 1 [23].

Figure 1. Concentration of oxygen (blue) and bubble radius (red). Bubble nucleates (r > 0) when gas has reached nucleation concentration. Reproduced with permission from [23].
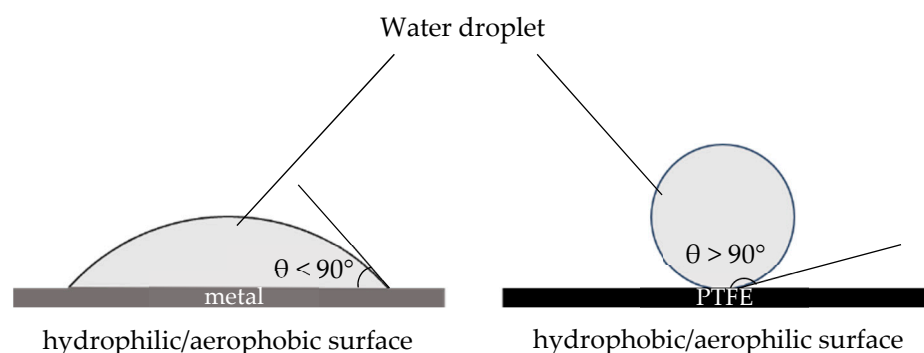
Bubbles grow until they reach detachment size. The bubble radius (i.e., bubble size) at detachment is determined by a mechanical force balance, including buoyancy, pressure, drag, inertia, capillary, and lift forces, as well as the size of the nucleation site [23]. In Figure 2, a bubble at the surface of one electrode in a vertical setup of the electrolysis cell is shown. When the buoyancy forces overcome the interfacial tension force (at the interface between the bubble and nucleation site), the bubble is said to have reached detachment size [26]. Thereafter, it will detach from the nucleation site and travel toward the electrolyte surface and out of the inter-electrode space due to buoyancy, overcoming adhering forces that are present upon the bubble. On the nucleation site, another bubble will form [23].

Figure 2. Schematic view of vertically positioned electrode with bubble attached (dashed-line circle) and released bubble (full-line circle) after some time. After the bubble reaches detachment size, it detaches due to buoyancy forces overcoming adhering forces. Produced according to [23,26].
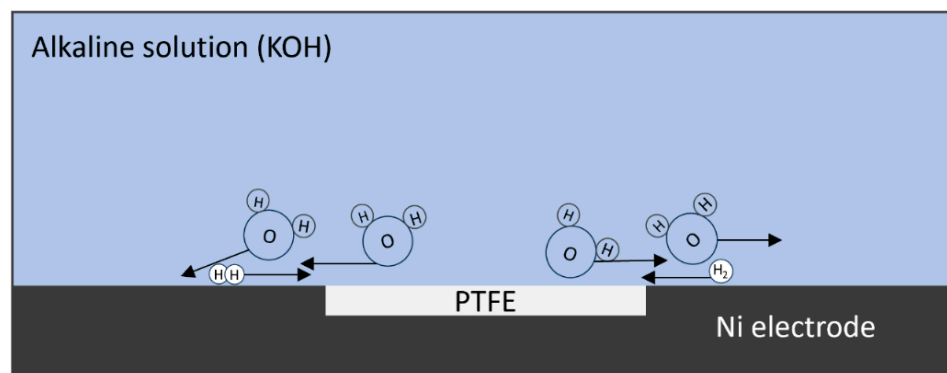
Previous studies have shown that bubble management has a significant effect on gas-generating catalytic reactions and consequently on the efficiency of water electrolysis [27]. The term 'bubble management' may include bubble-removing methods, such as mechanical convection, sonication, pressure modulation, the application of magnetic fields, or modifications to the wettability of the catalytic surface by making it superhydrophilic or superhydrophobic. The latter two effects may be used either to avoid bubble attraction (by reducing the liquid–solid interface contact angle) or promote preferential bubble nucleation (by directing bubble formation to specific controlled sites on the electrode surface) [20,28].

One bubble management strategy that has previously been examined involves creating "hydrophobic islands" on an electrode surface. This approach exploits surface tension (or free surface energy), which is a term used to describe the energy needed to increase the surface area of an object (or material) [29]. Surface tension is governed by its cohesive forces. When a fluid is brought into contact with an object, their surfaces interact and the force imbalance at both surfaces decrease; that is, the free surface energy of both surfaces is reduced. The degree of this reduction depends on how significant the interaction with the new neighbouring molecules is and determines whether the interfacial surface area of the fluid with the object will increase or not. It also determines how much it will increase. This process describes the 'wettability' of a surface or material. When, for example, a solid surface interacts very favourably with a water (fluid) surface, a hydrophilic/aerophobic surface with a contact angle of <90° is created, as depicted in Figure 3 (left), wherein the surface is strongly wetted by the fluid. By contrast, if the surface repels the fluid (water), then a hydrophobic/aerophilic surface with a contact angle of >90° is created, as depicted in Figure 3 (right) [29]. The wettability of the surface depends on the balance of the cohesive forces at the interface and the adhering forces inside the fluid.

Figure 3. Schematic depiction of a water droplet on a hydrophilic/aerophobic surface with contact angle θ < 90° (**left**) and a hydrophobic/aerophilic surface with contact angle θ > 90° (**right**). Adapted and reproduced with permission from [29].

The **Marangoni effect** is a phenomenon that occurs when materials with different surface tensions interact with each other. It describes, amongst others, the mechanics of attraction between the surface of a hydrophobic material such as the polymer poly(tetrafluoroethylene) (PTFE; or Teflon) and a gas bubble, which is also intrinsically hydrophobic [29–31]. While an exact analysis of the mechanics on the micro- and nanoscopic level is very complex and non-trivial, an approach based on surface tension theory and interfacial phenomena can be taken, as schematically shown in Figure 4.

Figure 4. Marangoni effect on a Ni electrode with a PTFE 'island' coated on it. Water molecules, which are hydrophilic, are repelled by and move away from PTFE to higher surface tension regions, while gas bubbles (or molecules), which are also hydrophobic, are attracted to and move toward the PTFE island. Reproduced referring to the theory described in [29,30].

In an aqueous solution, a hydrophobic material with a low surface tension (such as PTFE) creates a region of low surface tension around it. Materials with a similarly low surface tension (e.g., gas molecules or bubbles) are strongly attracted toward the PTFE surface, while hydrophilic materials are repelled by it [30]. By contrast, a hydrophilic surface will tend to attract hydrophilic molecules or materials and repel hydrophobic ones. That is, when there is a significant difference in surface tension at the interface, the material with the higher surface tension will increase the surface area of the material with the lower surface tension.

According to these principles, water molecules will tend to move away from a region of low surface tension in the vicinity of the PTFE surface to a region with higher surface tension, for example, the metallic surface of an electrode, following a surface tension gradient where wetting properties are better [29,31]. On the other hand, low-surface-tension hydrogen molecules dissolved in the solution, as well as hydrogen bubbles formed on the electrode surface, will tend to be displaced by water molecules as the degree of attraction between the metallic electrode surface and water, which is much higher than with a gas [30]. Simultaneously, the degree of attraction between PTFE and hydrogen molecules and bubbles is very high, leading to hydrogen gas and bubbles moving toward the PTFE surface. Through this mechanism, gas bubble formation can be directed away from the electrode surface and onto a PTFE island present on that surface, thereby minimizing the negative effects of bubbles on its surface [18,29]. As a result, the Ni electrode's active surface area remains free for gas-generating reactions to take place while the gas bubbles form on the surface of the PTFE island.

Bubble nucleation may also preferentially occur at the PTFE–electrode interface, where an increase in bubble coverage and size has been observed [19]. As has been described by the mathematical model of Kadyk and colleagues [23], the mass transport of gas into the bubbles diminishes the likelihood of gas concentrations in the liquid electrolyte reaching supersaturation levels, which decreases the concentration overpotential.

While there has not been intensive research on the effects of hydrophobic islands on electrolysis, several studies have confirmed their influence on the performance of electrolytic cells. Teschke and Galembeck [18] demonstrated that the presence of PTFE

islands on a cathode can have a beneficial effect on the electrode performance for the hydrogen evolving reaction (HER) by limiting activation and ohmic losses (overpotential) at current densities above 10 mA/cm^2, while at lower current densities, they had a negative effect. They found that at an optimal 20% PTFE coverage of the electrode (randomly dot-coated with PTFE islands), there was an overvoltage reduction of around ~0.15 V. Heidrich and Müller [19], on the other hand, observed a smaller improvement with their model with a maximum overvoltage decline of ~8 mV. Interestingly, they found that bubble coverage increased significantly on PTFE-coated samples and therefore allowed gas diffusion into the bubbles. They came to the conclusion that this led to a reduction in the concentration overpotential, contrary to the findings of Teschke and Galembeck. Other studies [28,32] have examined the influence and dynamic effects of bubble coalescence on bubble formation as well as on detachment size.

In this work, we have studied electrochemically induced hydrogen bubble formation on a nickel electrode surface coated with lines of PTFE. The impact of the PTFE line size (width) and degree of coverage was examined and analyzed. No improvement in the electrical energy efficiency for gas generation was observed up to 15 mA/cm^2 when comparing the PTFE-coated electrodes with the control bare uncoated electrode. However, increasing the PTFE coverage up to 15% generally improved electrolysis performance. Moreover, samples with 50% wider lines performed better (at the equivalent PTFE coverage), yielding an overpotential decline of up to 3.9% depending on the PTFE coverage. A 'bubble-scavenging' phenomenon was also observed, wherein bubbles observed to be present on the PTFE lines shrunk rapidly until they disappeared.
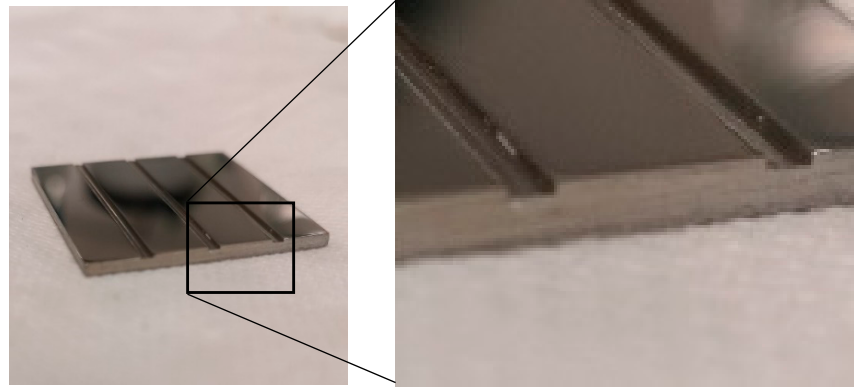
2. Materials and Methods

For this work, nickel (Ni) 200 plate electrodes with an area of 900 mm^2 (30 × 30 mm) were used as the working electrodes (WEs). The surface of the electrodes was covered with 'lines' of PTFE, wherein the overall area of the electrode covered with PTFE was 2%, 7%, or 15%; these percentages are referred to herein as the 'coverage' of PTFE applied. The PTFE was applied as lines having two different widths, namely a 1 mm width or 1.5 mm width. The performance of the working electrodes thus coated were compared with a bare uncoated electrode, which is referred to herein as the control electrode with 0% PTFE coverage. The methodology used in this work was developed and based on practices described previously.
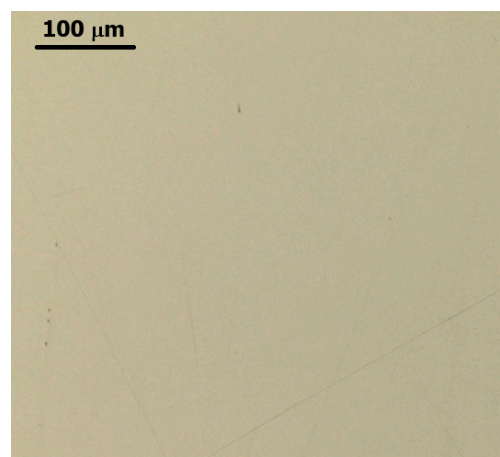
2.1. Electrode Preparation

For the PTFE deposition onto the electrode surface, a highly effective method was developed at the laboratories of the University of Wollongong. Linear grooves of different (desired) sizes were put onto the electrode surface using a milling/CNC machine (shown in Figure 5). The length of the grooves was calculated for every corresponding width and PTFE coverage. The electrodes were labelled in the format 'c%_xmm', where c is the coverage and x is the line width. For example, an electrode with a 7% PTFE coverage and a 1.5 mm PTFE line width was labelled as '7%_1.5 mm'. An exception was made for the 7%_1 mm electrode. To examine the impact of 1 mm-wide lines across the electrode, two lines of 30 × 1 mm were applied, which resulted in a coverage of 6.67%. For the sake of simplicity, this electrode will still be referred to as '7%_1 mm'. The margin of error was considered in the evaluation of the results if it was of significance. A groove depth of 0.34 mm was chosen for attachment stability of the PTFE on the electrodes.

The initial rough surface of the blank electrode was initially polished to achieve a mirror finish and to remove all visible cracks or crevices. Multiple steps of polishing were applied, starting with the use of silicon carbide (*SiC*) sandpaper of P500 grit, followed by P800, P1200, and P2000, each applied for 2:30 min. Thereafter, the electrodes were polished with alumina suspensions of 3 μm and 1 μm for 5 min and 10 min, respectively, producing the mirror-finish surface shown in Figure 6. Since roughness and crevices play a significant role on bubble formation and determine where it takes place, this

treatment of the electrode surface ensured that all electrodes had the same roughness with no edges present from crevices on the surface (visible to the bare eye) [26]. The resulting surface roughness Sq (root mean square height) was 0.058 μm measured using a 3D laser microscope.

Figure 5. Results of milling machine engraving of 1.5 mm-wide lines, each with a depth of 0.34 mm. The lines were later filled with PTFE, given an electrode with PTFE lines upon its surface.
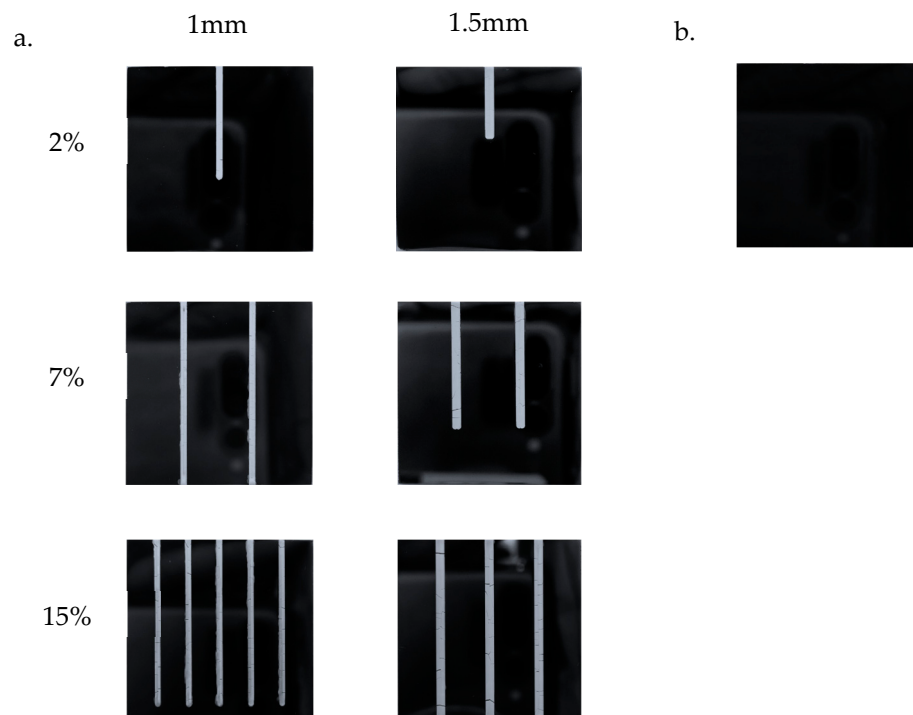

Figure 6. A 3D laser microscope image of the electrode surface after the polishing procedure. Tiny scratches of nm thickness are visible.

To remove any organic and other materials off the surface, all samples were immersed in isopropanol alcohol (IPA) and ultrasonicated for 15 min. After the ultrasonication, the electrodes were dried and PTFE dispersion of liquid form (60 wt.% in H_2O; Sigma-Aldrich sourced from Bayswater, Australia; contains 10 to 20% polyethylene glycol trimethyl-nonyl ether) was deposited in the grooves using a 25 G needle (0.50 × 25 mm). The deposition was possible due to capillary forces. The PTFE was left to dry (polymerize) at room temperature.

The resulting samples were heated for 6 h in a 40 L, 5-shelf, forced air convection oven at 200 °C to cause the binding of the PTFE with the electrode surface, thereby creating mechanical stability. After the heating procedure, the samples were left to cool to room temperature. The samples were kept in a desiccator until they were used to prevent oxidation and contact with air moisture. Figure 7 depicts the samples that were prepared.

Figure 7. (**a**) PTFE-coated samples after heat treatment, showing the overall percentage of coverage with PTFE of the left; (**b**) control bare electrode sample after heat treatment.

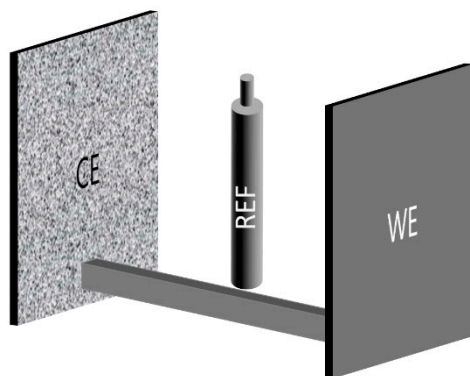## 2.2. Measurement of the Overall 'Coverage'

Measurement of the of PTFE coverage on the samples was performed using image processing and analysis with ImageJ software (version 1.53k). A photograph of the sample was taken and saved as a 32 bit image. The threshold of the image was adjusted to the point where the PTFE lines were filled with red (Figure 8). As a result, the coverage could be determined as the ratio of the red pixels to the total number of pixels in the image. All samples had a margin of error in the coverage no greater than 5%, with the lowest accuracy shown in the low coverages of 2%, which had an accuracy of 95%.

Figure 8. Photograph and image analysis (pixelation) to determine PTFE coverage using the program ImageJ. The photograph was adjusted until the PTFE line was filled with a red color, whereafter the ratio of red pixels to all pixels gave the PTFE coverage of the entire image.
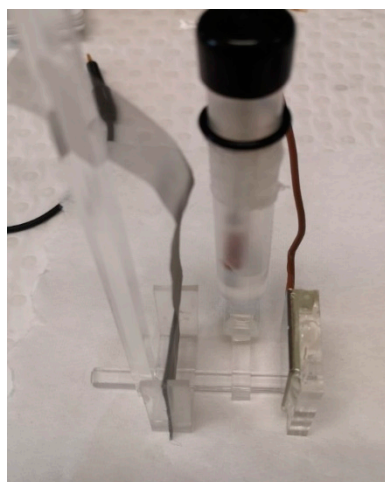
2.3. Electrochemical Setup

The working electrodes (WEs), as described above, were tested in a vertical disposition in a testing apparatus that was immersed in a 6 M KOH liquid electrolyte, as shown in Figure 9. A Ni mesh with a size of 40 × 180 mm was used as the counter electrode (CE). The Ni mesh was folded four times to a size of 40 × 45 mm, creating four layers of the Ni mesh, in order to ensure that the WE was current-limiting at all times. The preparation of the CE Ni mesh involved 15 min of ultrasonication in IPA, followed by immersion in 5 M HCl (=16 wt.% in H_2O) for 10 min. The purpose of the HCl treatment was to remove any oxide present on the Ni mesh surface.

Figure 9. Schematic view of 3-electrode setup of the cell (WE, CE, REF). The WE–CE distance was 30 mm with the REF in the middle, placed 15 cm from each electrode.

A 3-electrode setup was used for this work (WE, CE, and reference electrode), with the reference electrode (REF) being Hg/HgO. After placing the WE and CE electrodes in the vertical setup shown in Figure 9, the reference electrode (REF) was placed in the middle of the gap between the WE and the CE. The distance between the WE and CE was 30 mm. The cell was sealed with a lid and purged continuously with nitrogen (N_2) flow into the cell to eliminate any other gases present or entering the cell.

The cell assembly is shown in Figure 10. The cell was supported by a construction of a cut acrylic sheet. The WE was connected with a copper wire using a soldering device. To keep the WE fixed, it was attached with epoxy resin. The epoxy also served as an isolator of the back and the sides of the electrode, parts which do not participate in the reaction.

Figure 10. Electrochemical cell assembly.

During the chronopotentiometric electrochemical measurements, the very top of the WE was placed just above the surface of the liquid electrolyte for the reasons described below.

2.4. Electrochemical Measurements

All electrochemical measurements were carried out using a VSP biologic potentiostat/galvanostat. Chronopotentiometry (CP), cyclic voltammetry (CV) and current interrupt (CI) methods were used for the measurements.

To create a polarization curve, four current densities were chosen for each sample. To enable an accurate comparison and validation of the results between the samples, the same current density i [mA/cm^2] must be applied. Considering the different PTFE coverages of the samples, the electrochemically active area of the samples differs. Consequently, a

different current had to be applied for each sample so that the current density was the same for each sample, as shown in Table 1.

Table 1. Absolute applied currents for selected current densities and PTFE coverage.

Coverage c [%]	Current I for 2 mA/cm² [mA]	Current I for 5 mA/cm² [mA]	Current I for 10 mA/cm² [mA]	Current I for 15 mA/cm² [mA]
0 (bare)	18	45	90	135
2	17.64	44.1	88.2	132.3
7	16.74	41.85	83.7	125.55
15	15.3	38.25	76.5	114.75

Table 2 describes the entire experimental procedure, including all measurements with the corresponding duration, in chronological order. After fully immersing the cell in the electrolyte, it was purged for 10 min to remove any oxygen (O_2) present in the electrolyte and on the electrodes.

Table 2. Chronological order of the experiments undertaken during the electrochemical measurements.

Procedure/Measurement	Duration [min]
Purge	10
CV (20, 50, 100, 200 mV/s)	5
CI (3×)	1
Purge	5
CP (5×)	5 × 20
Purge (5×)	5 × 10

During the measurements, a flow of nitrogen was maintained just above the electrolyte surface (which here is called 'blanketing'). During purging, a flow of nitrogen was bubbled into the electrolyte. After the purging procedure, a set of CV (cyclic voltammetry) measurements (at scan rates of 20, 50, 100, and 200 mV/s) were carried out to determine the electrochemical active surface area (ECSA) of each electrode. This was followed by 3 repeated CI (current interrupt) resistance measurements. During the CI measurements, gas bubbles were produced by the electrodes and anchored on the electrode surface. To eliminate their influence on the following CI measurements, gas bubbles were eliminated by lifting the cell out of the electrolyte for 1 s. At the end of the third CI measurement, the cell was purged for 5 min.

This was followed by CP (chronopotentiometry) measurements repeated 5 times (quintuple repeats), which included 5 min of each of the four currents (2, 5, 10, 15 mA/cm²) which lasted 20 min in total. At the end of each CP run, the cell was lifted to get rid of the bubbles in the electrolyte and on the electrode surface, followed by 10 min of purging. As gas bubbles are still present in the electrolyte, they are attached to the electrode surface during the purging procedure. For this reason, the cell was lifted again for 1 s after 5 min of purging. This whole procedure was repeated five times for statistical evaluation.

Video recordings were created with the camera of a smartphone placed outside of the glass beaker (transparent color) containing the solution and the cell.

3. Results and Discussion

3.1. A Hypothesis That Was Tested

Figure 7a shows all the PTFE-coated electrodes prepared for this work. The control (bare) electrode is shown in Figure 7b. As can be seen, the PTFE lines started at the edge of the metal surface. This was deliberate, with the intention of leaving the top edge of the WE just above the surface of the liquid electrolyte. That is, the top edge of the PTFE line was made to lie just above the surface of the electrolyte solution and be exposed to and surrounded by the nitrogen blanket (N_2) that was maintained above it. We had speculated
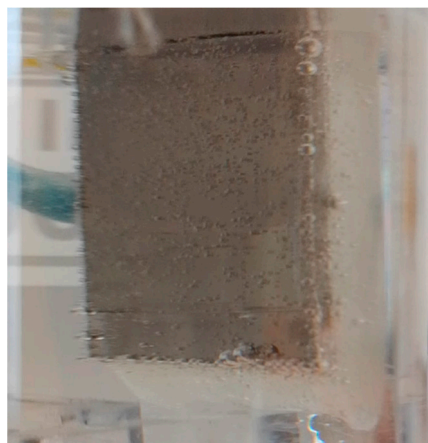
that according to the phenomena described above, when a bubble forms on the PTFE surface, it should be strongly attracted to it and form a relatively flat bubble (of the type depicted in Figure 3 (left)). It seemed possible that if multiple such flat bubbles formed on the surface of the PTFE lines, then they may coalesce, potentially providing a pathway for gas to travel up the PTFE line and exit above the surface of the liquid into the gaseous surroundings. One purpose of the work was to see whether a vertical setup of PTFE lines in contact with the gaseous atmosphere at its top edge would allow gas to be directly released to the gaseous blanket above the liquid surface in this way.

3.2. Optical Observations

Unfortunately, we did not observe gas generation that was unambiguously of this type. Discrete gas bubbles were generally observed to form on the PTFE lines, where they grew larger and moved upward due to buoyancy after release. However, we did observe a 'bubble-scavenging' phenomenon, wherein bubbles present on the PTFE lines appeared to shrink rapidly until they disappeared.

In the discussion below, we will first describe a typical sequence of bubble formation on the control bare electrode. We will then discuss and compare this to a typical sequence of events observed on an electrode coated with PTFE lines. Finally, we will describe the 'bubble-scavenging' phenomenon noted above.

Bubble formation on a bare electrode: Figure 11 shows a snapshot of a video recording taken during a CP run on the bare sample. Considering the flat and smooth electrode surface, no attached hydrogen bubbles were observed on the electrode. The bubbles shown in the picture were free-moving bubbles that quickly released and moved upward toward the water surface. However, attached static bubbles were observed on the edges of the electrode where the epoxy resin met the metallic surface and formed an interface. Additionally, some tiny parts of the electrode edges may have been left uncovered by the epoxy resin, which also strongly attracted bubbles.
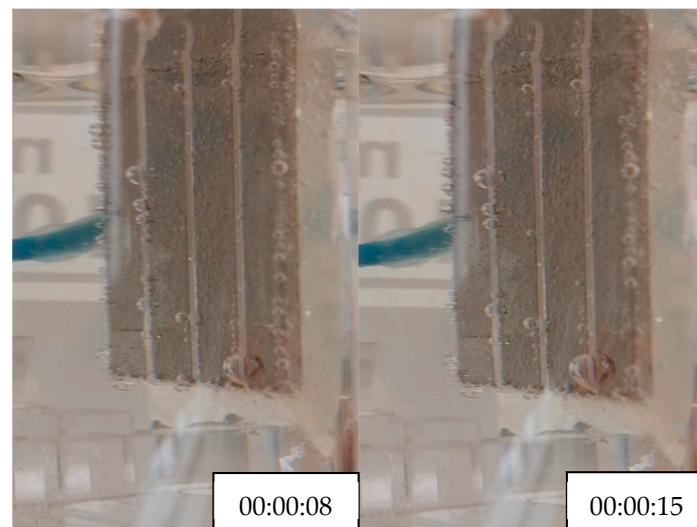

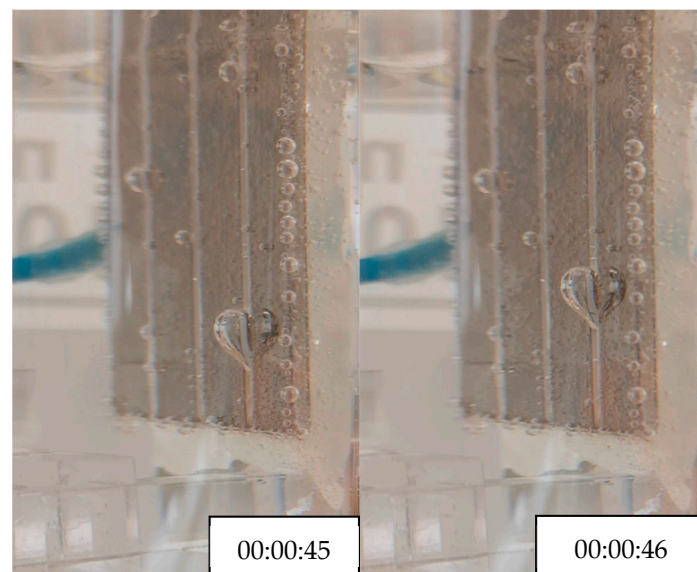**Figure 11.** Snapshot of video recording during CP run on bare uncoated electrode at 15 mA/cm^2.

Bubble formation on an electrode coated with PTFE lines: Figure 12 shows an image sequence of a recorded CP run on the 15%_1.5 mm electrode. Between 00:00:08 and 00:00:15, the bubble on the right PTFE line formed on the PTFE line and then grew larger due to gas transport into the bubbles or bubble coalescence while being attached to the PTFE line.

After 00:00:15, the bubble reached detachment size and started moving slowly upward along the PTFE line while its size continued to grow. As can be seen at 00:00:45 (Figure 13), the bubble became bigger and its shape changed due to buoyancy forces pushing it upward. At this point, the bubble moved faster and within 1 s (at 00:00:46), its position changed significantly compared to the previous sequence (00:00:45 in Figure 13), while its size did not change noticeably. In this way, the bubble was guided to the water surface and out

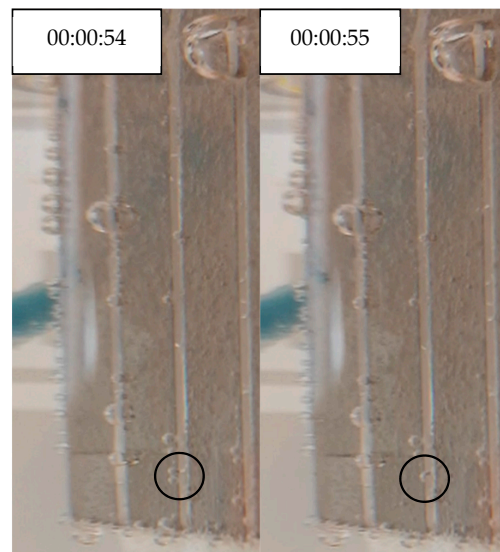of the inter-electrode space by the vertical PTFE line while still being attached along the PTFE line.

Figure 12. Image sequence (at 00:00:08 and 00:00:15 s) of CP run on 15%_1.5 mm sample. Bubble size grows.

Figure 13. Image sequence (at 00:00:45 and 00:00:46 s) of CP run on 15%_1.5 mm sample. Even after reaching detachment size, the bubble does not detach completely but stays attached on the PTFE line and travels along the line toward the electrolyte surface.

This could happen because of the Marangoni forces mentioned by Bashkatov et al. [28], where the adhering forces overcome buoyancy forces. It is important to note that static bubbles on the electrode edges at the epoxy resin interface were present on this and all other samples, as it was already shown for the bare electrode. Furthermore, other attached bubbles were observed at the electrode–PTFE interfaces.

The bubble attraction effect by the PTFE was also observed in the image sequence in Figure 14. At 00:00:54, two bubbles residing next to each other on the edge of the PTFE line at the Ni–PTFE interface coalesced into a single bigger bubble while they were spontaneously pulled by the PTFE at 00:00:55. This demonstrates that bubbles were attracted by the PTFE, removing them from the electrode surface.

Figure 14. Bubble coalescence onto the PTFE line of two bubbles sitting at the PTFE–Ni interface at second 00:00:54 and 00:00:55 (marked with black circles).

An unusual phenomenon was observed, however, at time points 00:00:56–00:00:57 (Figure 15). In a matter of one second, the bubble shown by the black circle in the 00:00:56 image shrank rapidly until it completely disappeared. It seemed to have been 'scavenged' by the PTFE. While we cannot say for sure what happened to the gas inside the bubble, the sequence of events could possibly be consistent with the bubble rapidly flattening, causing the gas to move upward, toward the liquid surface (since the top edge of the PTFE is in contact with the air). This could possibly be enabled by special (albeit undefined) conditions of the bubble and its vicinity, a strong attraction of the bubble to the PTFE, and the vertical positioning of the PTFE line, which together with the PTFE connected to the blanked gaseous atmosphere above the liquid, may conceivably have acted as a canal for the gas in the bubble to rapidly exit the inter-electrode space and the electrolyte.
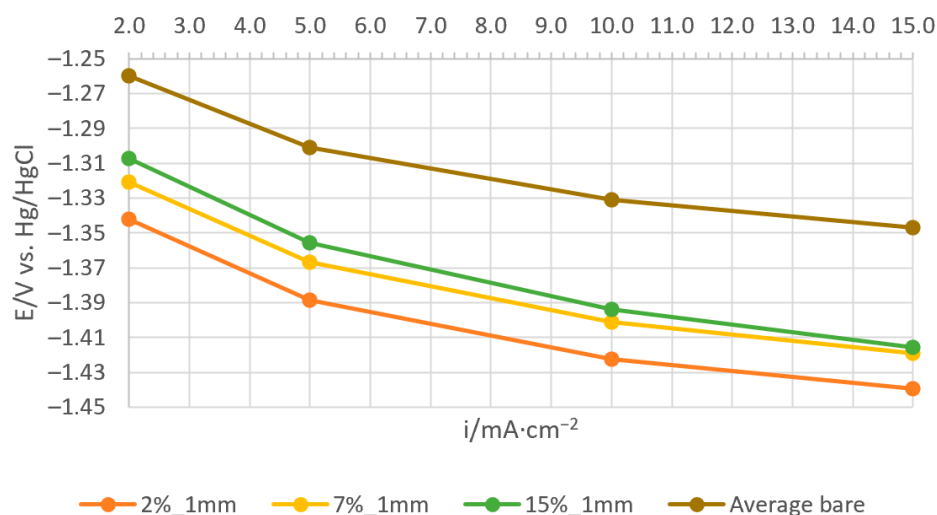

Figure 15. 'Bubble-scavenging' effect of the coalesced bubble on PTFE at second 00:00:56 and 00:00:57 (marked with black circles). The bubble is assumed to 'deflate' due to gas being removed toward the water surface along the PTFE line.

3.3. Polarization Curves

Figure 16 shows the polarization curves of the samples coated with 1 mm lines of PTFE (each of which was the average of the quintuplet repeats of the CP step) compared to the control bare electrode (the data for which were the result of the average of two measurements). All data were resistance-corrected via Hg/HgO. The measured potential for all four samples indicated that the presence of the 1 mm lines of PTFE on the Ni electrode did not improve the performance of the electrolysis when compared to the results of the bare electrode. That is, the bare electrode required a lower voltage (i.e., a less negative voltage) at all current densities than the PTFE-coated electrodes.
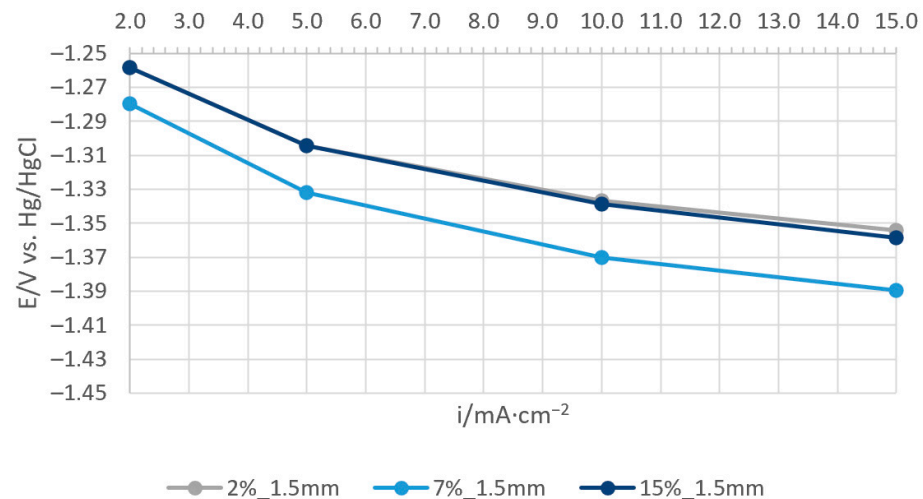

Figure 16. Polarization curves of samples coated with 1 mm PTFE lines (geometrical active area); CP.

There was, however, a clear trend based on the PTFE coverage. While the control bare electrode achieved potentials as low as ca. -1.26 V at 2 mA/cm^2 and ca. -1.33 V at 15 mA/cm^2, the best performing PTFE sample was the one with 15% coverage (15%_1 mm), achieving ca. -1.31 V at 2 mA/cm^2 and ca. -1.415 V at 15 mA/cm^2. The worst performing sample (2%_1 mm) required ca. -1.34 V at 2 mA/cm^2 and -1.44 V at 15 mA/cm^2. This shows that with an increasing PTFE coverage up to 15%, the performance of the PTFE samples and the efficiency of hydrogen production increased.

Coating the Ni electrode with 1.5 mm-wide PTFE lines produced a better overall performance compared to the 1 mm lines, as shown in Figure 17. In that case, all of the PTFE-coated samples performed essentially identically to the uncoated bare control, except for the 7%_1.5 mm sample. Thus, despite the reduced active surface area of the PTFE samples, they produced gas as efficiently as the bare uncoated electrode (except for 7%_1.5 mm). The 15%_1.5 mm sample produced 2 mA/cm^2 at ca. -1.26 V—almost performing the same as the bare electrode. At 15 mA/cm^2, the 15%_1.5 mm samples required -1.36 V. Compared to the 15%_1 mm sample, this is a decrease in voltage of around 3.8% and 3.9%, respectively. Likewise, the 7%_1.5 mm sample shows an improvement in efficiency compared to the 7%_1 mm sample, with a potential decrease of around 3% and 2.1%, respectively. These findings mean that the width of the PTFE lines played an important role in the electrolysis performance of the coated Ni electrode, a finding which adds to the study of Teschke and colleagues [18].

The performance of all samples (described in Figures 16 and 17) is shown for clear comparison in Table 3 among the samples coated with 1 mm-wide PTFE lines (Table 3a) and those coated with 1.5 mm-wide PTFE lines (Table 3b).

Figure 17. Polarization curves of samples coated with 1.5 mm PTFE lines (geometrical active area); CP.

Table 3. Measured voltage [V] for current densities 2, 5, 10, 15 mA/cm^2 of (**a**) samples coated with 1 mm-wide PTFE lines and (**b**) samples coated with 1.5 mm-wide PTFE lines.

(a)				
Current Density i [mA/cm^2]	PTFE Coverage (0%)	PTFE Coverage (2%)	PTFE Coverage (7%)	PTFE Coverage (15%)
2	−1.26	−1.34	−1.32	−1.31
5	−1.30	−1.39	−1.37	−1.36
10	−1.33	−1.42	−1.40	−1.39
15	−1.35	−1.44	−1.42	−1.41
(b)				
Current Density i [mA/cm^2]	PTFE Coverage (0%)	PTFE Coverage (2%)	PTFE Coverage (7%)	PTFE Coverage (15%)
2	−1.26	−1.26	−1.28	−1.26
5	−1.30	−1.30	−1.33	−1.30
10	−1.33	−1.34	−1.37	−1.34
15	−1.35	−1.35	−1.39	−1.36

4. Conclusions

This work sought to study novel gas-generating electrodes coated with new line patterns of Teflon (PTFE) in an attempt to reduce overpotentials produced in gas-generating electrochemical cells, thus increasing system efficiency.

This work was focused on the hydrogen evolving reaction (HER). Line patterns of 1 mm and 1.5 mm widths were used with three different overall coverages (2%, 7%, 15%). The performance in the hydrogen generation of the six samples was compared to an equivalent bare electrode. Furthermore, the cell was positioned vertically, and the top of the PTFE lines were placed in contact with the gaseous volume above the liquid. PTFE was deposited in and filled line grooves made on the surface of the electrode.

The depositing method for the PTFE lines proved to be highly accurate (ca. 95%) and varying widths and lengths of the line could be achieved. Wider lines had an overall better performance, as the samples with 1.5 mm-wide lines demonstrated less overpotential than the samples with 1 mm lines. When the width was increased by 50% (1.5 mm lines), the overpotential was reduced from 2.1% to 3.9% depending on the coverage degree. Overpotential also decreased with increasing PTFE coverage. As a result, the best performing sample was the one coated with 1.5 mm lines and 15% PTFE coverage, which performed almost the same as the control bare electrode. However, none of the samples performed better than the control bare electrode.

Optical observations were made. Hydrogen bubbles at the PTFE–Ni interface were attracted to and moved onto the PTFE due to Marangoni forces. As the bubbles increased in size, they constantly moved upward (due to buoyancy forces) along the PTFE lines with increasing speed, without being detached until they exited the inter-electrode space. This shows that PTFE lines in a vertical setup can very well assist in guiding attached bubbles to desired directions. Some bubbles were also attracted by the PTFE and rapidly shrunk until they disappeared in a matter of seconds. This phenomenon was called 'bubble-scavenging', as the bubbles seemed to disappear on the PTFE. The governing forces and mechanism responsible for this 'bubble-scavenging' phenomenon are non-trivial and should be studied further to be understood. Further research including samples with higher coverage and various PTFE sizes (width) should be carried out to establish the influence of line patterns on the bubbles and electrolysis performance.

References

1. Kovač, A.; Paranos, M.; Marciuš, D. Hydrogen in energy transition: A review. *Int. J. Hydrogen Energy* **2021**, *46*, 10016–10035. [CrossRef]
2. Bhandari, R.; Shah, R.R. Hydrogen as energy carrier: Techno-economic assessment of decentralized hydrogen production in Germany. *Renew. Energy* **2021**, *177*, 915–931. [CrossRef]
3. World Energy Council. *World Energy Trilemma Index 2020*; IAEA: France, 2020.
4. Pfeifer, A.; Krajačić, G.; Ljubas, D.; Duić, N. Increasing the integration of solar photovoltaics in energy mix on the road to low emissions energy system—Economic and environmental implications. *Renew. Energy* **2019**, *143*, 1310–1317. [CrossRef]
5. Ibrahim, H.; Ilinca, A.; Perron, J. Energy storage systems—Characteristics and comparisons. *Renew. Sustain. Energy Rev.* **2008**, *12*, 1221–1250. [CrossRef]
6. Sun, Y.; Zhao, Z.; Yang, M.; Jia, D.; Pei, W.; Xu, B. Overview of energy storage in renewable energy power fluctuation mitigation. *CSEE J. Power Energy Syst.* **2020**, *6*, 160–173.
7. Koohi-Fayegh, S.; Rosen, M. A review of energy storage types, applications and recent developments. *J. Energy Storage* **2020**, *27*, 101047. [CrossRef]
8. Hossain, E.; Faruque, H.M.R.; Sunny, M.S.H.; Mohammad, N.; Nawar, N. A Comprehensive Review on Energy Storage Systems: Types, Comparison, Current Scenario, Applications, Barriers, and Potential Solutions, Policies, and Future Prospects. *Energies* **2020**, *13*, 3651. [CrossRef]
9. Małachowska, A.; Łukasik, N.; Mioduska, J.; Gębicki, J. Hydrogen Storage in Geological Formations—The Potential of Salt Caverns. *Energies* **2022**, *15*, 5038. [CrossRef]
10. Carmona-Martinez, A.A.; Fresneda-Cruz, A.; Rueda, A.; Birgi, O.; Khawaja, C.; Janssen, R.; Davidis, B.; Reumerman, P.; Vis, M.; Karampinis, E.; et al. Renewable Power and Heat for the Decarbonisation of Energy-Intensive Industries. *Processes* **2023**, *11*, 18. [CrossRef]
11. Rambhujun, N.; Salman, M.S.; Wang, T.; Pratthana, C.; Sapkota, P.; Costalin, M.; Lai, Q.; Aguey-Zinsou, K.-F. Renewable hydrogen for the chemical industry. *MRS Energy Sustain.* **2020**, *7*, E33. [CrossRef]
12. Gray, N.; McDonagh, S.; O'Shea, R.; Smyth, B.; Murphy, J.D. Decarbonising ships, planes and trucks: An analysis of suitable low-carbon fuels for the maritime, aviation and haulage sectors. *Adv. Appl. Energy* **2021**, *1*, 100008. [CrossRef]
13. Egeland-Eriksen, T.; Hajizadeh, A.; Sartori, S. Hydrogen-based systems for integration of renewable energy in power systems: Achievements and perspectives. *Int. J. Hydrogen Energy* **2021**, *46*, 31963–31983. [CrossRef]
14. Pellow, M.A.; Emmott, C.J.M.; Barnhardt, C.J.; Benson, S.M. Hydrogen or batteries for grid storage? A net energy analysis. *Energy Environ. Sci.* **2015**, *8*, 1938–1952. [CrossRef]
15. Salonen, L.; Petrovykh, D.; Kolen, Y. Sustainable catalysts for water electrolysis: Selected strategies for reduction and replacement of platinum-group metals. *Mater. Today Sustain.* **2021**, *211*, 100060. [CrossRef]

16. Kibsgaard, J.; Chorkendorff, I. Considerations for the scaling-up of water splitting catalysts. *Nat. Energy* **2019**, *4*, 430–433. [CrossRef]

17. Communication from The Commission to The European Parliament, the Council, the European Economic and Social Committee and The Committee of the Regions—Critical Raw Materials Resilience: Charting a Path towards Greater Security and Sustainability. Available online: https://ec.europa.eu/docsroom/documents/42849 (accessed on 2 September 2024).

18. Teschke, O.; Galembeck, F. Effect of PTFE Coverage on the Performance of Gas Evolving Electrodes. *J. Electrochem. Soc.* **1984**, *131*, 1095–1097. [CrossRef]

19. Heidrich, H.-J.; Müller, L. The effect of hydrophobic centres on the electrode surface on overvoltage in electrochemical gas evolution. *Electrochim. Acta* **1990**, *35*, 1089–1093.

20. Swiegers, G.F.; Terrett, R.N.L.; Tsekouras, G.; Tsuzuki, T.; Paceb, R.J.; Stranger, R. The prospects of developing a highly energyefficient water electrolyser by eliminating or mitigating bubble effects. *Sustain. Energy Fuels* **2021**, *5*, 1280–1310. [CrossRef]

21. Li, J.; Zhu, Y.; Chen, W.; Lu, Z.; Xu, J.; Pei, A.; Peng, Y.; Zheng, X.; Zhang, Z.; Chu, S.; et al. Breathing-Mimicking Electrocatalysis for Oxygen Evolution and Reduction. *Joule* **2019**, *3*, 557–569. [CrossRef]

22. Hodges, A.; Renz, S.; Lohmann-Richters, F.; Al-Musawi, A.; Jupke, A.; Lehnert, W.; Swiegers, G.F.; Wallace, G.G. Critical Analysis of Published Physical Property Data for Aqueous Potassium Hydroxide. Collation into Detailed Models for Alkaline Electrolysis. *J. Chem. Eng. Data* **2023**, *68*, 1485–1506. [CrossRef]

23. Kadyk, T.; Bruce, D.; Eikerling, M. How to Enhance Gas Removal from Porous Electrodes? *Sci. Rep.* **2016**, *6*, 38780. [CrossRef] [PubMed]

24. German, S.R.; Edwards, M.A.; Ren, H.; White, H.S. Critical Nuclei Size, Rate, and Activation Energy of H_2 Gas Nucleation. *J. Am. Chem. Soc.* **2018**, *140*, 4047–4053. [CrossRef] [PubMed]

25. Ren, H.; German, S.R.; Edwards, M.A.; Chen, Q.; White, H.S. Electrochemical Generation of Individual O_2 Nanobubbles via H_2O_2 Oxidation. *J. Phys. Chem. Lett.* **2017**, *8*, 2450–2454. [CrossRef] [PubMed]

26. Angulo, A.; Linde, P.V.D.; Gardeniers, H.; Modestino, M.; Rivas, D.F. Influence of Bubbles on the Energy Conversion Efficiency of Electrochemical Reactors. *Joule* **2020**, *4*, 555–579. [CrossRef]

27. Tiwari, P.; Tsekouras, G.; Wagner, K.; Swiegers, G.F.; Wallace, G.G. A new class of bubble-free water electrolyzer that is intrinsically highly efficient. *Int. J. Hydrogen Energy* **2019**, *44*, 23568–23579. [CrossRef]

28. Bashkatov, A.; Park, S.; Demirkır, C.; Wood, J.A.; Koper, M.T.M.; Lohse, D.; Krug, D. Performance Enhancement of Electrocatalytic Hydrogen Evolution through Coalescence-Induced Bubble Dynamics. *J. Am. Chem. Soc.* **2024**, *146*, 10177–10186. [CrossRef]

29. Rapp, B.E. *Chapter 20—Surface Tension, in Microfluidics: Modeling, Mechanics and Mathematics*; Elsevier: New York, NY, USA, 2017; pp. 421–444.

30. Van Oss, C.J. *Interface Science and Technology*; Elsevier: New York, NY, USA, 2008; Volume 16, pp. 149–160.

31. Schmitt, M.; Stark, H. Marangoni flow at droplet interfaces: Three-dimensional solution and applications. *Phys. Fluids* **2016**, *28*, 012106. [CrossRef]

32. Brussieux, C.; Viers, P.; Roustan, H.; Rakib, M. Controlled electrochemical gas bubble release from electrodes entirely and partially covered with hydrophobic materials. *Electrochim. Acta* **2011**, *56*, 7194–7201. [CrossRef]